Acta Crystallographica Section F
Structural Biology and Crystallization Communications
ISSN 1744-3091

Expression, purification and crystallization of the Cmi immunity protein from *Escherichia coli*

Christin Römer, Silke I. Patzer, Reinhard Albrecht, Kornelius Zeth* and Volkmar Braun

Department for Protein Evolution, Max Planck Institute for Developmental Biology, Spemannstrasse 35, D-72076 Tübingen, Germany

Correspondence e-mail: kornelius.zeth@tuebingen.mpg.de

Received 31 August 2010
Accepted 22 February 2011

Many bacteria kill related bacteria by secretion of bacteriocins. In *Escherichia coli*, the colicin M protein kills *E. coli* after uptake into the periplasm. Self-protection from destruction is provided by the co-expressed immunity protein. The colicin M immunity protein (Cmi) was cloned, overexpressed and purified to homogeneity. The correct fold of purified Cmi was analyzed by activity tests and circular-dichroism spectroscopy. Crystallization trials yielded crystals, one of which diffracted to a resolution of 1.9 Å in the orthorhombic space group $C222_1$. The crystal packing, with unit-cell parameters a = 66.02, b = 83.47, c = 38.30 Å, indicated the presence of one monomer in the asymmetric unit with a solvent content of 53%.

1. Introduction

Colicins are protein toxins encoded on plasmids of certain *Escherichia coli* strains. They kill *E. coli* cells by pore formation in the cytoplasmic membrane, DNA and RNA hydrolysis or by inhibiting murein (peptidoglycan) and O-antigen biosynthesis. Each of the 20 well studied colicins from *E. coli* has its own inactivating immunity protein. Immunity proteins protect producer cells against the colicin that they form by binding to the colicins (Cascales *et al.*, 2007).

Colicin M (Cma) is active in the periplasm and cleaves the phosphate-ester bond between the murein precursor and lipid II, resulting in C_{55} polyisoprenol, which no longer translocates the murein and O-antigen precursors from the cytoplasm into the periplasm, where they are incorporated into murein and lipopolysaccharide (Schaller *et al.*, 1982; Harkness & Braun, 1989*a*,*b*; El Ghachi *et al.*, 2006). The inhibition of murein biosynthesis results in cell lysis (Braun *et al.*, 1974). We recently determined the crystal structure of Cma and found that the phosphatase has no structural similarity to known phosphatases, which agrees with its lack of sequence homology to any known phosphatases (Zeth *et al.*, 2008). Cma producer cells are protected by the colicin M immunity protein Cmi. The *cmi* gene is located adjacent to the *cma* activity gene on pColBM plasmids (Olschläger & Braun, 1987) and is co-transcribed with *cma*. Cmi is anchored to the periplasmic surface of the cytoplasmic membrane (Gross & Braun, 1996) where the substrate of Cma is localized.

Previous and current attempts to determine the binding affinity of Cmi for active Cma released from cells resulted in only very weak binding (Gross & Braun, 1996; Olschläger *et al.*, 1991; C. Römer, unpublished work). Consequently, the mechanism by which Cmi inactivates Cma is not known. To understand the mechanism of inactivation, Cmi was produced and crystallized and crystallographic studies were conducted.

2. Materials and methods

2.1. Construction of plasmids

The *cmi* gene was amplified by PCR from pPG105 (Gross & Braun, 1996) with oligonucleotides synthesized by Eurofins MWG Operon (Ebersberg, Germany) and Phusion polymerase (Finnzymes, Espoo, Finland). The product was cloned into the blunted *Nde*I/*Xho*I sites of the pET22b expression vector (Merck Chemicals, Bad Soden, Germany). The resulting plasmid pSP130/42 encodes Cmi(Δ1–23) (Swiss-Prot P18002, amino acids 48–141) with an additional starting

methionine and a C-terminal His tag (residues LEHHHHHH). To prepare the protein for expression in the periplasm, *blaT'-'cmi* on pPG775 (Gross & Braun, 1996) was amplified by PCR and cloned into the blunted *Nde*I/*Xho*I sites of pET22b. The resulting plasmid pSP130/39 encodes the signal sequence of BlaT (MSIQHFRVALI-PFFAAFCLPVFA), Cmi(Δ1–23) and the C-terminal His tag LEH-HHHHH. The constructs were confirmed by DNA sequencing.

2.2. Overexpression and purification

E. coli BL21 (DE3) cells transformed with plasmid pSP130/39 or pSP130/42 were grown in 4.8 l LB medium supplemented with ampicillin (50 µg ml^{-1}) at 310 K with shaking. At an OD_{578} of 0.5, 1 m*M* isopropyl *β*-D-1-thiogalactopyranoside (IPTG) was added and growth continued for 3 h. The cells were spun down at 277 K and suspended in 10 ml buffer *A* (Zeth *et al.*, 2008) containing 1 mg ml^{-1} DNAse. The cells were disrupted using a French press and cell debris was removed by centrifugation. The supernatant was filtered through fibreglass (0.45 µm) and then subjected to affinity chromatography on a 50 ml Ni–NTA agarose column as described previously for Cma purification (Zeth *et al.*, 2008). The eluted fractions were examined by SDS–PAGE for the presence of Cmi(Δ1–23) and contaminating proteins. For crystallization, the final buffer of the Ni–NTA chromatography was exchanged for 20 m*M* Tris–HCl, 50 m*M* NaCl pH 7.4 by dialysis for 2 d. The resulting protein was concentrated to a concentration of 5.3 mg ml^{-1} by centrifugation using an Amicon 3K filter.

Figure 1
Purified Cmi(Δ1–23) (right lane) used in crystallography. The left lane shows the sizes of standard proteins (kDa).

2.3. Circular-dichroism (CD) spectroscopy

CD measurements were performed on a Jasco J-810 spectropolarimeter (Jasco, Gross-Umstadt, Germany) equipped with a thermoelectric temperature controller. Spectra were recorded with a 1 mm quartz cuvette at 190–250 nm using a bandwidth of 1 nm, a scanning speed of 100 nm min^{-1}, a data pitch of 0.2 nm, a response time of 1 s and accumulation of at least five spectra. Thermal denaturation was monitored at 218 nm between 283 and 368 K with a temperature ramp of 1 K min^{-1} and a data pitch of 0.5 K. Single spectra were taken at 283, 293, 303, 313, 323, 333, 343, 353 and 363 K. The *Spectra Manager* 2 software was used for data processing, subtraction of the buffer baseline, calculation of the melting temperature and the prediction of secondary structure. Measurements were performed at a concentration of 15 µ*M* Cmi(Δ1–23) in 25 m*M* Tris–HCl pH 7.5.

The melting temperature was determined in the range 304–368 K under the following conditions: fitting line of stable range, *A* $y = -0.00940378x - 9.02818$, *B* $y = 0.021272x - 21.6364$; residual of fitting curve, $\sigma = 0.040011$; $T_m = 339.78 \pm 0.152442$ K; $\Delta H = -91374.9 \pm 1931.29$ J mol^{-1}; $\Delta S = -268.927 \pm 5.68401$ J mol^{-1} K^{-1}.

2.4. Crystallization and crystallographic analysis

For crystallization, 0.4 µl purified Cmi(Δ1–23) in 20 m*M* Tris, 50 m*M* NaCl pH 7.4 was mixed with 0.4 µl reservoir solution on 96-well Intelli-Plates (Art Robbins) using a Honeybee 961 robot

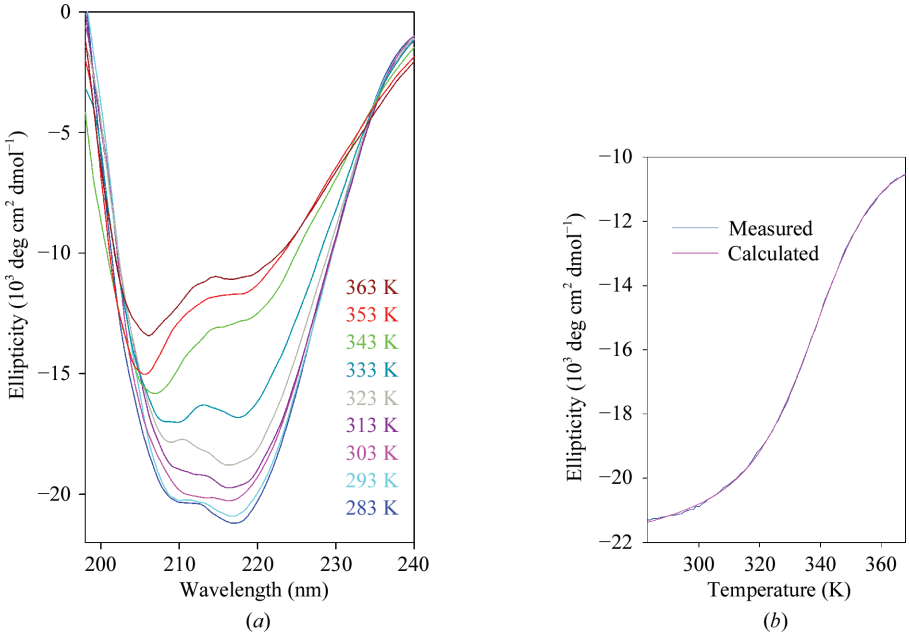

Figure 2
(*a*) CD spectra of Cmi(Δ1–23) at the indicated temperatures and (*b*) fitting of the determined melting curve to the calculated melting curve with $T_m = 339.78$ K.

Table 1
Crystallographic analysis of the Cmi(Δ1–23) crystal.

Values in parentheses are for the highest resolution shell.

Beamline	PX10, SLS
CCD detector	MAR 225
Crystal dimensions (μm)	200 × 50 × 50
Space group	$C222_1$
Unit-cell parameters	
a (Å)	66.02
b (Å)	83.57
c (Å)	38.30
Resolution limits (Å)	50–1.89 (2.00–1.89)
Wavelength (Å)	0.9789
Oscillation angle (°)	1
Observed reflections	41344
Unique reflections	15884
Completeness (%)	96.6 (90.0)
Multiplicity	2.6 (2.5)
$\langle I/\sigma(I)\rangle$	10.9 (2.5)
$R_{\rm merge}$†	0.078 (0.507)

† $R_{\rm merge} = \sum_{hkl}\sum_i |I_i(hkl) - \langle I(hkl)\rangle| / \sum_{hkl}\sum_i I_i(hkl)$, where $I_i(hkl)$ is the intensity of reflection *hkl* and $\langle I(hkl)\rangle$ is the average intensity of reflection *hkl*.

(Genomic Solutions) and 13 different crystal screens (Qiagen), giving a total of 1248 conditions. The plates were stored at 293 K. Drops were imaged 1, 7 and 30 d after setup using a Rock Imager 54 system (Formulatrix). Images were inspected for crystal formation. One needle-shaped crystal appeared between the first and the seventh day after setup in condition F9 of the PEG II screen (0.2 *M* ammonium sulfate, 30% PEG 4000). The crystal was picked up in a small nylon loop (Hampton Research), briefly immersed in reservoir solution supplemented with 10% ethylene glycol and immediately flash-frozen in liquid nitrogen.

2.5. Data collection and processing

X-ray data were collected on beamline PXII at the Swiss Light Source (SLS, Villigen, Switzerland). The diffraction experiment was conducted at 100 K and images were recorded on a 225 mm MAR CCD camera (MAR Research). A resolution of 1.9 Å was achieved. Data were indexed, integrated and scaled using the programs *XDS* and *XSCALE* (Kabsch, 2010).

Figure 3
Crystal of Cmi(Δ1–23) used for X-ray analysis. The scale bar represents a length of 200 μm.

3. Results and discussion

The immunity protein Cmi inactivates Cma after uptake into the periplasm. To unravel the inactivation mechanism, we set out to analyze the Cmi structure by X-ray crystallography. The actual translation product of the *cmi* gene is shorter than listed in the data bank of *E. coli* genomes. It starts at the third methionine (residue 25; Olschläger *et al.*, 1991), which is followed by a 23-residue hydrophobic sequence through which Cmi is anchored to the cytoplasmic membrane (Olschläger & Braun, 1987).

To avoid the use of detergents in purification, the N-terminal hydrophobic membrane anchor was omitted and the truncated protein, Cmi(Δ1–23), was cloned with a C-terminal His tag into *E. coli* BL21 (DE3). Addition of IPTG to the growth culture resulted in production of the protein, which was further purified by Ni–NTA chromatography to finally yield the pure protein as judged by a single protein band on SDS–PAGE (Fig. 1). Cmi(Δ1–23) protected cells from being killed by externally added Cma, as described previously (Gross & Braun, 1996); the addition of the His tag did not inactivate Cmi.

To further characterize the native state of Cmi(Δ1–23), CD spectra were recorded at different temperatures (Fig. 2). Since we occasionally observed N-terminal truncation of cytoplasmic Cmi, a second clone was constructed which secreted Cmi into the periplasm, where it was stable. The thermally induced Cmi unfolding characteristics revealed an approximate melting point $T_{\rm m}$ of 339.8 K. The spectra indicate that at the temperature used for crystallization Cmi was in a native state, which is also supported by the inactivation of Cma. The secondary structure was predicted to be ∼50% β-sheets, 10% α-helices, 5% turns and 30–40% random structure.

The purified protein was submitted to crystallization trials and we succeeded in obtaining a crystal using a solution consisting of 0.2 *M* ammonium sulfate, 30% polyethylene glycol 4000 (Fig. 3). The crystal diffracted to a resolution of 1.9 Å (Fig. 4). The protein crystallized in

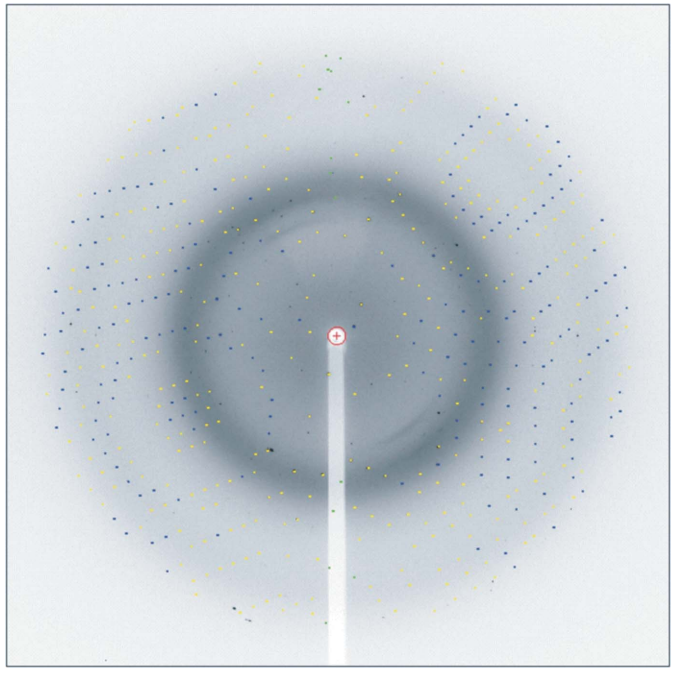

Figure 4
Diffraction pattern of the Cmi(Δ1–23) crystal, which diffracted to a resolution of 1.9 Å. Diffraction spots were recorded on a MAR 225 CCD image plate. Spots are encircled using the *MOSFLM* software for better visibility (Leslie, 1992).

space group $C222_1$, with one monomer in the asymmetric unit and a solvent content and Matthews coefficient of 53% and 2.35 Å^3 Da^{-1}, respectively (Table 1). A protein-sequence search against the sequences in the PDB (as of July 2010) revealed no similar protein structures as a putative search model, which is indicative of a potentially novel fold of the protein. Currently, we are trying to solve the structure by a combination of MIR and MAD techniques using protein crystals for heavy-atom soaking and protein labelling by selenomethionine using the two natural methionines.

We thank Dr Andrei Lupas and the Max Planck Society for generous support and Kerstin Bär for setup of the crystallization drops. We also thank the staff of beamline PXII, SLS, Villigen for help and beamline maintenance.

References

Braun, V., Schaller, K. & Wabl, M. R. (1974). *Antimicrob. Agents Chemother.* **5**, 520–533.
Cascales, E., Buchanan, S. K., Duché, D., Kleanthous, C., Lloubès, R., Postle, K., Riley, M., Slatin, S. & Cavard, D. (2007). *Microbiol. Mol. Biol. Rev.* **71**, 158–229.
El Ghachi, M., Bouhss, A., Barreteau, H., Touzé, T., Auger, G., Blanot, D. & Mengin-Lecreulx, D. (2006). *J. Biol. Chem.* **281**, 22761–22772.
Gross, P. & Braun, V. (1996). *Mol. Gen. Genet.* **251**, 388–396.
Harkness, R. & Braun, V. (1989*a*). *J. Biol. Chem.* **264**, 6177–6182.
Harkness, R. & Braun, V. (1989*b*). *J. Biol. Chem.* **264**, 14716–14722.
Kabsch, W. (2010). *Acta Cryst.* D**66**, 125–132.
Leslie, A. G. W. (1992). *Jnt CCP4/ESF–EACBM Newsl. Protein Crystallogr.* **26**.
Olschläger, T. & Braun, V. (1987). *J. Bacteriol.* **169**, 4765–4769.
Olschläger, T., Turba, A. & Braun, V. (1991). *Mol. Microbiol.* **5**, 1105–1111.
Schaller, K., Höltje, J. V. & Braun, V. (1982). *J. Bacteriol.* **152**, 994–1000.
Zeth, K., Römer, C., Patzer, S. I. & Braun, V. (2008). *J. Biol. Chem.* **283**, 25324–25331.